New Journal of Physics
The open-access journal for physics

Spin–orbit coupling and conservation of angular momentum flux in non-paraxial imaging of forbidden radiation

Matthew R Foreman and Peter Török
Blackett Laboratory, Department of Physics, Imperial College London, Prince Consort Road, London SW7 2BZ, UK
E-mail: matthew.foreman@imperial.ac.uk and peter.torok@imperial.ac.uk

New Journal of Physics **13** (2011) 063041 (9pp)
Received 1 April 2011
Published 23 June 2011
Online at http://www.njp.org/
doi:10.1088/1367-2630/13/6/063041

Abstract. Rigorous, closed form expressions are derived for non-paraxial imaging of sources of multipole radiation from which conservation of angular momentum (AM) flux is established. Coupling of spin and orbital optical AM flux is also quantitatively investigated, highlighting the importance of spin–orbit interactions in high numerical aperture imaging.

Contents

1. Introduction

Radiation from atoms or molecules arises through electron transitions; however, quantum selection rules dictate that many such transitions are forbidden under an electric dipole approximation. So-called forbidden radiation can nevertheless still be emitted via electric dipole forbidden transitions due to higher order multipole corrections to the transition matrix, such as the magnetic dipole or electric quadrupole coupling terms. Despite the inherent lower transition probabilities, sources of forbidden radiation now play a greater role in much of today's science.

One such example is use of the $4S$ to $3D$ transition in $^{43}Ca^{+}$ ions for realization of ion-based quantum computers, since here longer radiative lifetimes are desirable [1]. Multiphoton transitions, important in nonlinear microscopy and spectroscopy applications alike [2, 3], are by virtue of angular momentum (AM) conservation also sources of higher order multipole radiation [4]. On a more macroscopic level it has furthermore long been known that extended sources (i.e. ones for which their largest dimension $> \lambda$) give rise to high order multipole contributions to the radiated field distributions [5]. More recently, subwavelength nano-antennas have also been shown to produce complicated far field distributions due to plasmonic effects [6].

Routinely, sources of radiation (be they forbidden or not) are studied by use of an imaging system [2, 7], yet a rigorous treatment of such a scenario is hitherto absent from the literature. Consequently, a full understanding of measured data is similarly lacking, which can lead to inaccurate interpretations or large errors. Detection from different directions has, for example, been shown to exhibit significantly different properties in both the near and the far field due to the directionality of multipole sources [8, 9]. To compound matters, high numerical aperture (NA) optics are frequently employed, so as to provide the resolution required, hence necessitating full electromagnetic models to account for polarization effects. This paper therefore presents recent analytic results in this vein. One potential application of this work is thus development of high sensitivity readout modalities in, for example, quantum computing, biological imaging and material/lithographic inspection.

Multipole radiation and AM are fundamentally related [5] and it is difficult to consider one without mentioning the other. Within an optical context AM has itself received extensive investigation, motivated primarily by the seminal work of Allen *et al* [10]. Recent efforts have been both experimental and theoretical, with advances made in each domain (see [11] for a collection of relevant works). Experimental work has, for instance, concerned the generation of beams with AM and the optical manipulation and trapping of atoms and particles. On the other hand, theoretical endeavours have predominantly studied separation of AM into spin and orbital components (SAM and OAM, respectively). Paraxial beams, quite naturally allow for this separation, where OAM is carried by helical phase fronts of the form $e^{im\phi}$ (m is known as the topological charge of a beam), while SAM is carried by circularly polarized light. Conceptual difficulties, however, arise for non-paraxial systems since a mixing of OAM and SAM arises [12, 13], due to the spin–orbit interaction of light [14]. To overcome such mixing in non-paraxial systems Barnett proposed use of AM flux instead [15], leading to a definition of separable SAM and OAM flux components. Interchange between SAM and OAM (and flux) is a similar coupling effect that has drawn considerable attention, particularly in tight optical focusing [16–18]. Investigation and quantification of the SAM and OAM flux exchange (SOE) in non-paraxial imaging naturally follows from the multipole formalism developed here and a number of results are hence also presented. Such studies allows fundamental insights to be gained into the properties of light and optical systems. Within a polarization domain, knowledge of the inter-component polarization mixing arising from high NA lenses, allowed advances in superresolution, material processing and optical manipulation [19]. It is hence conceivable that similar possibilities may be afforded by exploiting AM interchange.

2. Imaging theory

Any well-corrected single lens used as an imaging device may be represented as a double lens system arranged in a $4f$ configuration, whereby the lenses are placed such that their foci

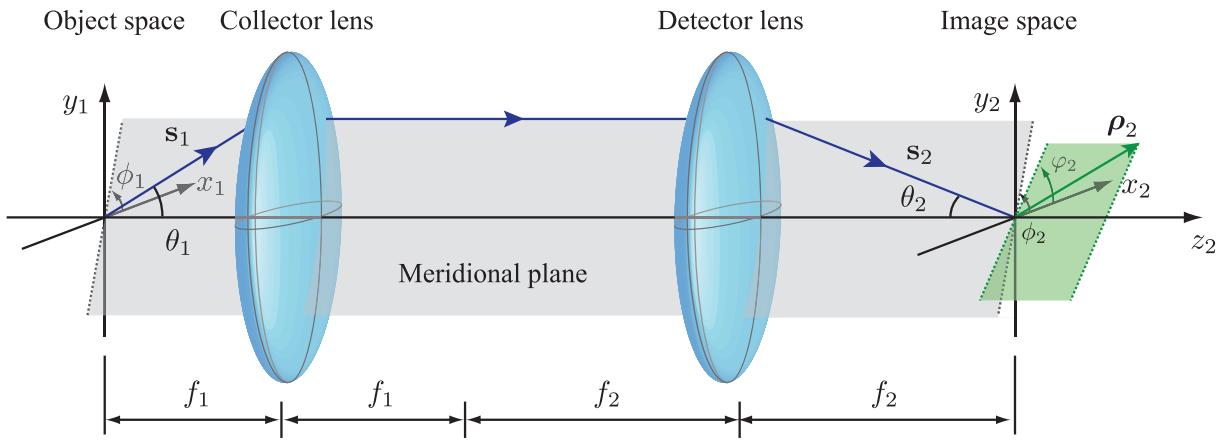

Figure 1. $4f$ telecentric imaging setup used to image multipole sources. Object and image plane positions are defined by the vectors $\boldsymbol{\rho}_1$ and $\boldsymbol{\rho}_2$, respectively, while positions on the reference spheres associated with the collector and detector lenses (with $\mathrm{NA}_1 = \sin\alpha_1$ and $\mathrm{NA}_2 = \sin\alpha_2$) are defined by the coordinates (θ_1, ϕ_1) and (θ_2, ϕ_2).

coincide. More complex optical setups can in turn be modelled as a combination of one or more lens pairs [20], such that fundamentally only imaging through a $4f$ system need be considered. Critically, introduction of an aperture stop in the common focal plane yields an afocal and telecentric system from both object and image spaces, such that vectorial ray tracing can be used to compute the image field [21].

Consider then the action of the imaging system on a plane wave, originating in the object space, travelling in a direction $\mathbf{s}(\theta_1, \phi_1) = (\sin\theta_1\cos\phi_1, \sin\theta_1\sin\phi_1, \cos\theta_1)$ and with associated generalized (3×1) Jones vector $\mathbf{E}(\theta_1, \phi_1)$ (see figure 1). Each lens in the system rotates the polarization vector of the ray about an axis perpendicular to the meridional plane in which it propagates, as can be treated using a generalized Jones matrix formalism [21]. The geometric field distribution on the Gaussian reference sphere of the focusing lens, assuming a transmission geometry, for a single ray is hence

$$\widetilde{\mathbf{E}}_2(\theta_2, \phi_2) = \frac{a(\theta_2)}{a(\theta_1)}\mathbb{R}_z^{-1}(\phi_1)\mathbb{R}_y(-\theta_2)\mathbb{R}_y(-\theta_1)\mathbb{R}_z(\phi_1)\widetilde{\mathbf{E}}_1(\theta_1, \phi_1), \tag{1}$$

where $a(\theta)$ is an apodization factor ($= \sqrt{\cos\theta}$ for an aplanatic lens) required to conserve energy at each lens and $\mathbb{R}_\mu(\alpha)$ denotes a rotation of α about the μ coordinate axis [21]. Note (θ_2, ϕ_2) define the direction of propagation of the ray in image space.

Devaney and Wolf have however given the angular spectrum of multipole radiation of order (l, m) as [22]

$$\begin{bmatrix} \widetilde{E}^v_{lm,r}(\theta,\phi) \\ \widetilde{E}^v_{lm,\theta}(\theta,\phi) \\ \widetilde{E}^v_{lm,\phi}(\theta,\phi) \end{bmatrix} = C_{lm}(-i)^l\,\mathrm{e}^{\mathrm{i}m\phi} \begin{bmatrix} 0 \\ \Theta^v_{lm}(\theta) \\ \Phi^v_{lm}(\theta) \end{bmatrix}, \tag{2}$$

where $\nu = \mathrm{E(M)}$ denotes an electric (magnetic) multipole, $C_{lm} = [(2l+1)(l-m)!]^{1/2}/[4\pi(l+m)!]^{1/2}$ and

$$\Theta^{\mathrm{E}}_{lm}(\theta) = \mathrm{i}\frac{\partial}{\partial\theta}P^m_l(\cos\theta) = -\Phi^{\mathrm{M}}_{lm}(\theta),$$
$$\Phi^{\mathrm{E}}_{lm}(\theta) = -\frac{m}{\sin\theta}P^m_l(\cos\theta) = \Theta^{\mathrm{M}}_{lm}(\theta).$$

Here, $P^m_l(\cos\theta)$ are the associated Legendre polynomials. Rewriting equation (2) in terms of Cartesian field components allows direct substitution into equation (1), yielding

$$\widetilde{\mathbf{E}}^{\nu}_{lm,2}(\theta_2,\phi_2) = C_{lm}(-i)^l\,\mathrm{e}^{\mathrm{i}m\phi}\frac{a(\theta_2)}{a(\theta_1)}\begin{bmatrix}\Theta^{\nu}_{lm}(\theta_1)\cos\theta_2\cos\phi_1 - \Phi^{\nu}_{lm}(\theta_1)\sin\phi_1\\ \Theta^{\nu}_{lm}(\theta_1)\cos\theta_2\sin\phi_1 + \Phi^{\nu}_{lm}(\theta_1)\cos\phi_1\\ -\Theta^{\nu}_{lm}(\theta_1)\sin\theta_2\end{bmatrix}.$$

The final image field $\mathbf{E}(\boldsymbol{\rho}_2)$ at a position $\boldsymbol{\rho}_2$ relative to the geometric image point for a monochromatic field of wavelength λ, can then be found using the Debye–Wolf [23] integral, originally formulated by Ignatowsky [24],

$$\mathbf{E}^{\nu}_{lm}(\boldsymbol{\rho}_2) = -\frac{\mathrm{i}f_2}{\lambda}\int_0^{2\pi}\int_0^{\alpha_2}\widetilde{\mathbf{E}}^{\nu}_{lm,2}(\theta_2,\phi_2)\mathrm{e}^{\mathrm{i}kz_2\cos\theta_2}$$
$$\times\exp\left[\mathrm{i}k\rho_2\sin\theta_2\cos(\phi_2-\varphi_2)\right]\sin\theta_2\,\mathrm{d}\theta_2\,\mathrm{d}\phi_2,$$

where (ρ_2,φ_2,z_2) are the cylindrical polar coordinates of $\boldsymbol{\rho}_2$, while f_2 and α_2 are the focal length and semi-angle of convergence of the focusing lens respectively and $k = 2\pi/\lambda$. Using the identity [25]

$$\int_0^{2\pi}\mathrm{e}^{\mathrm{i}n\beta}\exp[\mathrm{i}a\cos(\beta-\gamma)]\mathrm{d}\beta = 2\pi\mathrm{i}^n\mathrm{e}^{\mathrm{i}n\gamma}J_n(a),$$

where $J_n(a)$ is the nth order Bessel function of the first kind, the azimuthal integration can be performed analytically, yielding

$$\mathbf{E}^{\nu}_{lm}(\boldsymbol{\rho}_2) = \frac{C_{lm}\pi f_2}{\lambda}i^{m-l-1}\begin{bmatrix}\mathrm{i}E_{m+1}K^{+\nu}_{lm} - \mathrm{i}E_{m-1}K^{-\nu}_{lm}\\ E_{m+1}K^{+\nu}_{lm} + E_{m-1}K^{-\nu}_{lm}\\ -2E_mK^{0\nu}_{lm}\end{bmatrix},$$

where $E_n = \exp[in\varphi_2]$, $f_1\sin\theta_1 = f_2\sin\theta_2$ and

$$K^{\pm\nu}_{lm} = \int_0^{\alpha_2}\frac{a(\theta_2)}{a(\theta_1)}\left[\Theta^{\nu}_{lm}(\theta_1)\cos\theta_2 \pm \mathrm{i}\Phi^{\nu}_{lm}(\theta_1)\right]\sin\theta_2,$$
$$\times J_{m\pm1}(k\rho_2\sin\theta_2)\exp\left[\mathrm{i}k(z_2\cos\theta_2 - z_{\mathrm{mp}}\cos\theta_1)\right]\mathrm{d}\theta_2,$$

$$K^{0\nu}_{lm} = \int_0^{\alpha_2}\frac{a(\theta_2)}{a(\theta_1)}\Theta^{\nu}_{lm}(\theta_1)\sin^2\theta_2$$
$$\times J_m(k\rho_2\sin\theta_2)\exp\left[\mathrm{i}k(z_2\cos\theta_2 - z_{\mathrm{mp}}\cos\theta_1)\right]\mathrm{d}\theta_2.$$

The extra term $z_{\mathrm{mp}}\cos\theta_1$ has been introduced to the exponent to allow lateral displacements of the multipole source. Transverse shifts to a position $\boldsymbol{\rho}_{\mathrm{mp}}$ can further be incorporated, assuming shift invariance of the imaging system such that $\mathbf{E}^{\nu,\mathrm{off\text{-}axis}}_{lm}(\boldsymbol{\rho}_2) = \mathbf{E}^{\nu,\mathrm{on\text{-}axis}}_{lm}\left(\boldsymbol{\rho}_2 - [f_2/f_1]\boldsymbol{\rho}_{\mathrm{mp}}\right)$. Using the curl equations it can similarly be shown that the associated magnetic field distributions

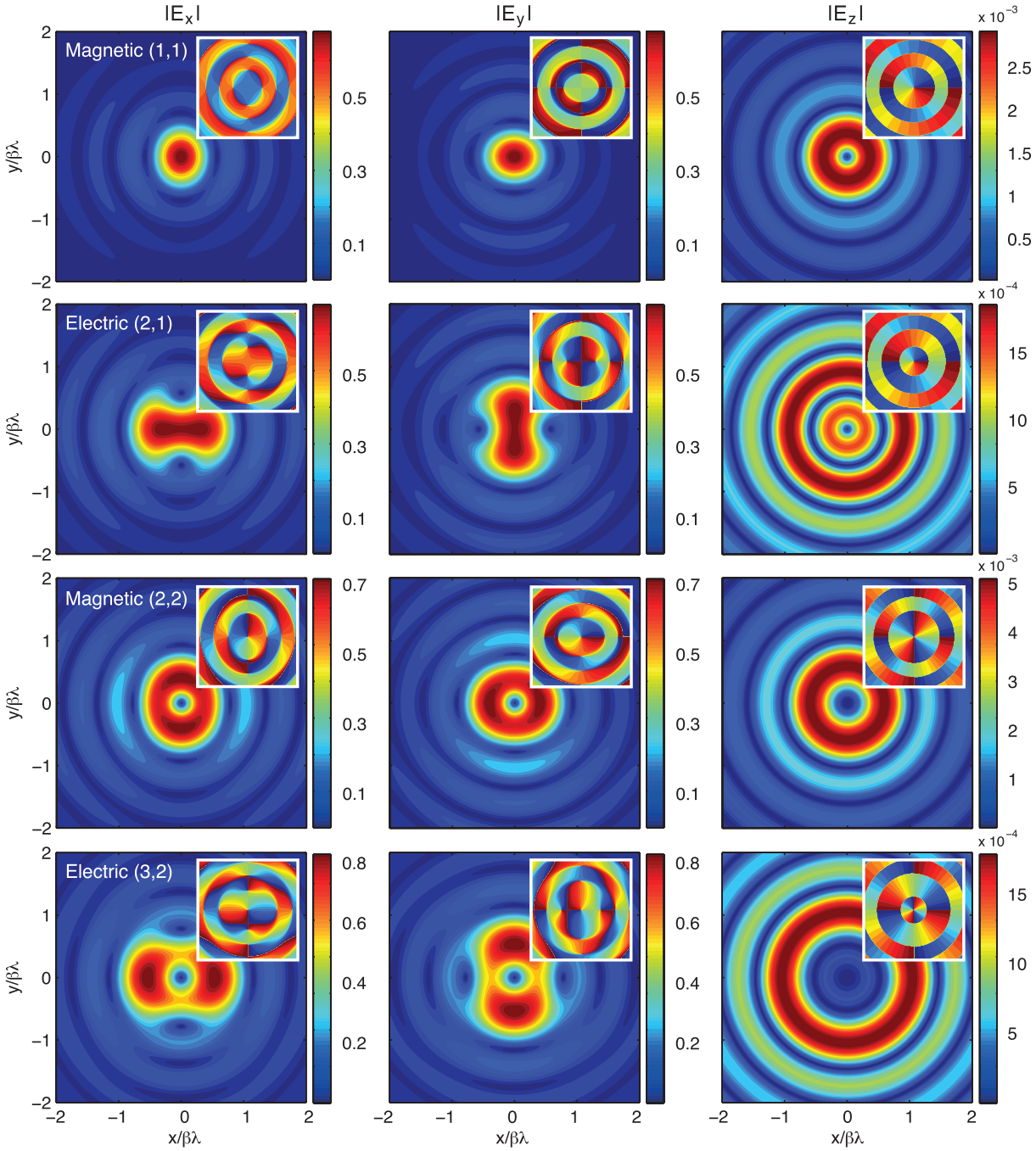

Figure 2. Left to right: Amplitude and phase (inset) distributions of Cartesian electric field components (E_x, E_y, E_z), in the image plane ($z_2 = 0$) of a high NA $4f$ system, imaging electric and magnetic multipole sources of order (l, m). Phase plots run from $-\pi$ (blue) to π (red).

are $\mathbf{B}^{\nu}_{lm}(\boldsymbol{\rho}_2) = \pm\mathbf{E}^{\bar{\nu}}_{lm}(\boldsymbol{\rho}_2)/c$, where the positive sign is taken for $\nu = M$, c is the speed of light and $\bar{\nu} = \mathrm{E}$ if $\nu = \mathrm{M}$ and vice versa.

Figure 2 shows the calculated field distributions (amplitude and phase) in the image plane of a $4f$ imaging system ($100\times$) in which the collector lens has a NA of 0.95, for assorted

electric and magnetic multipoles. Azimuthally periodic phase distributions are clearly evident, suggesting the presence of OAM. It is furthermore interesting to note that due to the form of the $K_{lm}^{\pm\nu}$ and $K_{lm}^{0\nu}$ integrals, zero total energy density is always seen on axis when imaging multipole radiation with $|m| > 1$.

3. Angular momentum (AM) flux

Following Barnett's definition [15], the total AM flux density (3×3) tensor is defined here as $\mathbb{M} = \boldsymbol{\rho} \times \mathbb{T}$, such that $M_{ij} = \sum_{mn} \epsilon_{imn} \rho_m T_{nj}$, where $\mathbb{T}$ is Maxwell's electromagnetic stress tensor and ϵ_{imn} is the Levi–Civita symbol. Restricting to time harmonic fields of angular frequency ω and performing cycle averages, the elements of Maxwell's stress tensor are given by

$$T_{ij} = \frac{\delta_{ij}}{4}\left[\varepsilon_0|\mathbf{E}|^2 + \frac{1}{\mu_0}|\mathbf{B}|^2\right] - \frac{\varepsilon_0}{2}\Re[E_i E_j^*] - \frac{1}{2\mu_0}\Re[B_i B_j^*],$$

where δ_{ij} is the Kronecker delta, such that the flux of the z-component of the OAM and SAM in the z-direction is respectively

$$M_{zz}^{\text{orbit}} = \frac{\varepsilon_0 c^2}{4\omega}\Im\left[E_y\frac{\partial B_x^*}{\partial\varphi_2} - B_x^*\frac{\partial E_y}{\partial\varphi_2} + B_y^*\frac{\partial E_x}{\partial\varphi_2} - E_x\frac{\partial B_y^*}{\partial\varphi_2}\right],$$

$$M_{zz}^{\text{spin}} = \frac{\varepsilon_0 c^2}{2\omega}\Im\left[E_x B_x^* + E_y B_y^*\right].$$

In general, these fluxes are a function of position $\boldsymbol{\rho}_2$, however this dependance has been dropped for clarity. The integrated flux $\mathcal{M}_{zz}$ through a plane of constant z, can then be shown to be

$$\mathcal{M}_{zz}^{\text{orbit}} = \mathcal{M}_0\,\Im\left[\int_0^\infty \left\{K_{lm}^{-\nu}K_{lm}^{-\bar{\nu}*} + K_{lm}^{+\nu}K_{lm}^{+\bar{\nu}*}\right\}\rho_2\,\mathrm{d}\rho_2\right], \tag{3}$$

$$\mathcal{M}_{zz}^{\text{spin}} = \mathcal{M}_0\,\Im\left[\int_0^\infty \left\{(m-1)K_{lm}^{-\nu}K_{lm}^{-\bar{\nu}*} - (m+1)K_{lm}^{+\nu}K_{lm}^{+\bar{\nu}*}\right\}\rho_2\,\mathrm{d}\rho_2\right], \tag{4}$$

where $\mathcal{M}_0 = \pm\pi^2 C_{lm}^2 \varepsilon_0 f_2^2/\lambda$ and the azimuthal integration has again been performed analytically. Integrated fluxes of the x- and y-component of AM through a fixed transverse plane is zero by symmetry. Symmetry in the kernels furthermore ensures that $\mathcal{M}_{zz}^{\text{orbit}} = \mathcal{M}_{zz}^{\text{spin}} = 0$ when $m = 0$. Similarly, an integrated energy flux through a fixed plane can be found by integrating the z-component of the Poynting vector, viz

$$\mathcal{F}_z = \omega\mathcal{M}_0\,\Im\left[\int_0^\infty \left\{K_{lm}^{-\nu}K_{lm}^{-\bar{\nu}*} - K_{lm}^{+\nu}K_{lm}^{+\bar{\nu}*}\right\}\rho_2\,\mathrm{d}\rho_2\right]. \tag{5}$$

Given equations (3)–(5) it quickly follows that

$$\mathcal{R}_1 = \frac{\mathcal{M}_{zz}^{\text{orbit}} + \mathcal{M}_{zz}^{\text{spin}}}{\mathcal{F}_z} = \frac{m}{\omega} = \frac{m\lambda}{2\pi c},$$

which holds regardless of which transverse plane is considered (mathematically this ratio holds for any surface which is rotationally symmetric with respect to the z-axis e.g. a hemisphere, although a transverse plane is of greater physical interest here). The ratio $\mathcal{R}_1$ can also be considered before imaging, i.e. in the object space of the multipole source, whereby the same

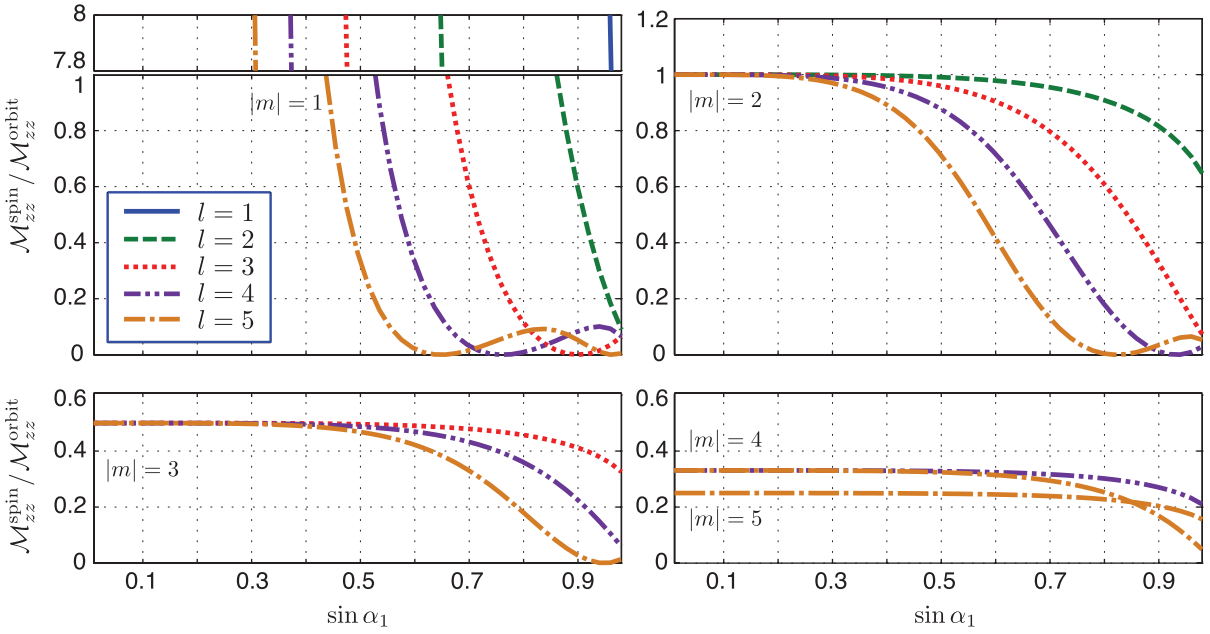

Figure 3. Dependance of the ratio of the integrated SAM and OAM flux in the z-direction, $\mathcal{M}_{zz}^{\text{spin}}/\mathcal{M}_{zz}^{\text{orbit}}$, on the NA of the collector lens $\sin\alpha_1$.

result holds. Evidently the ratio $\mathcal{R}_1$ is not only a conserved quantity upon propagation in both spaces, but is also preserved upon imaging.

Finally, it is worthwhile to investigate the relative magnitudes of the SAM and OAM flux in non-paraxial imaging systems. Accordingly, the ratio $\mathcal{R}_2 = \mathcal{M}_{zz}^{\text{spin}}/\mathcal{M}_{zz}^{\text{orbit}}$ is plotted in figure 3 for different multipole orders ($m \neq 0$) as a function of collector lens NA (letting $z_2 = 0$). These results are invariant with $\sin\alpha_2$, and hence also magnification of the imaging system. In the low NA limit ($\alpha_1 \to 0$) the SAM flux is always non-zero, accounting for a fraction of $1/|m|$ of the total AM flux in the z direction (or equivalently $\mathcal{F}_z/\omega$ or $\hbar$ per photon). In contrast, the OAM constitutes $\min(|m \pm 1|)$ of the total axial flux (in units of $\mathcal{F}_z/\omega$).

As the non-paraxiality of the system increases, so the relative proportion of SAM flux drops, ultimately to a value close to zero. Interestingly, the conversion of SAM flux to OAM flux for $l = 1$, $m = \pm 1$ multipoles is negligible with $\mathcal{R}_2 \gg 1$ at $\alpha_1 \sim \pi/2$. Observation of the SOE for these sources hence requires use of immersion lenses. As the order l is increased, the SOE progressively becomes more apparent with the drop off to zero of $\mathcal{R}_2$ occurring at lower NAs. Conversely, the reduction in SAM flux for higher $|m|$ sources occurs at higher NAs. Qualitatively, this behaviour can be understood by noting that uniformly polarized fields possess only SAM, such that OAM is introduced by breaking the uniformity. Lower l corresponds to less directional, and hence inherently more uniform, radiation patterns, which is only broken by the spatially dependent polarization mixing introduced by lenses of high NA. Higher $|m|$ furthermore implies that the direction of maxima in the radiation lobes form smaller angles with the z-direction, such that the field collected by the lens is more uniformly polarized. Consider for example a z oriented dipole ($l = 1$, $m = 0$) which gives rise to a (highly non-uniform) azimuthally polarized field distribution in the back focal plane of the collector lens, whilst the combination

of out of phase x- and y-oriented dipoles ($m = \pm 1$) yields a fairly uniform circularly polarized beam. Large $|m|$ sources hence again require higher NA lenses to introduce polarization mixing.

4. Conclusions

In summary, closed form rigorous electromagnetic results have been derived pertaining to the imaging of multipole sources of arbitrary order by a high NA $4f$ imaging system. Orbital, spin AM and energy fluxes have been calculated in the focal region, whereby it was shown that the ratio of the total integrated AM flux to energy flux in the z direction was a conserved quantity upon both propagation and imaging. The magnitude of the SOE in non-paraxial imaging was also quantitatively studied. Possible applications and future research directions founded on these results could include design and optimization of optical detection modalities based on the SOE, measuring sample induced spin–orbit interactions [26] or imaging of forbidden radiation. Consideration could also be given to more arbitrary sources represented by a superposition of multipoles. On a final note, it should be mentioned that although throughout this paper a classical treatment has been given, following the discussion in [15] the problem can equally be formulated in a quantum domain.

Acknowledgment

This work was supported by the European Union SURPASS project (Grant No. 224226).

References

[1] Stock R and James D F V 2009 Scalable, high-speed measurement-based quantum computer using trapped ions *Phys. Rev. Lett.* **102** 170501
[2] Duemani Reddy G, Kelleher K, Fink R and Saggau P 2008 Three-dimensional random access multiphoton microscopy for functional imaging of neuronal activity *Nat. Neurosci.* **11** 713–20
[3] Bushev P, Müller C, Lisenfeld J, Cole J H, Lukashenko A, Shnirman A and Ustinov A V 2010 Multiphoton spectroscopy of a hybrid quantum system *Phys. Rev.* B **82** 134530
[4] Docker M P 1988 Alignment measurements using one, two or three photons *Chem. Phys.* **125** 185–210
[5] Jackson J D 1998 *Classical Electrodynamics* (New York: Wiley)
[6] Kosako T, Kadoya Y and Hofmann H F 2010 Directional control of light by a nano-optical Yagi–Uda antenna *Nat. Photonics* **4** 312–5
[7] Nelson K D, Li X and Weiss D S 2007 Imaging single atoms in a three-dimensional array *Nat. Phys.* **3** 556–60
[8] Novotny L 1997 Allowed and forbidden light in near-field optics. II. Interacting dipolar particles *J. Opt. Soc. Am.* A **14** 105–13
[9] van de Nes A S and Török P 2007 Rigorous analysis of spheres in Gauss–Llaguerre beams *Opt. Express* **15** 13360–74
[10] Allen L, Beijersbergen M W, Spreeuw R J C and Woerdman J P 1992 Orbital angular momentum of light and the transformation of Laguerre–Gaussian laser modes *Phys. Rev.* A **45** 8185–9
[11] Allen L, Barnett S M and Padgett M J 2003 *Optical Angular Momentum* (Bristol: Institute of Physics)
[12] Monteiro P B, Maia Neto P A and Nussenzveig H M 2009 Angular momentum of focused beams: beyond the paraxial approximation *Phys. Rev.* A **79** 033830
[13] Martínez-Herrero R and Mejías P M 2010 Angular momentum decomposition of nonparaxial light beams *Opt. Express* **18** 7965–71

[14] Bliokh K Y, Alonso M A, Ostrovskaya E A and Aiello A 2010 Angular momenta and spin–orbit interaction of nonparaxial light in free space *Phys. Rev.* A **82** 063825
[15] Barnett S M 2002 Optical angular-momentum flux *J. Opt. B: Quantum Semiclass. Opt.* **4** S7
[16] Zhao Y, Edgar J S, Jeffries G D M, McGloin D and Chiu D T 2007 Spin-to-orbital angular momentum conversion in a strongly focused optical beam *Phys. Rev. Lett.* **99** 073901
[17] Nieminen T A, Stilgoe A B, Heckenberg N R and Rubinsztein-Dunlop H 2008 Angular momentum of a strongly focused gaussian beam *J. Opt. A: Pure Appl. Opt.* **10** 115005
[18] Braat J J M, van Haver S, Janssen A J E M and Dirksen P 2007 Energy and momentum flux in a high numerical aperture beam using the extended Nijboer-Zernike diffraction formalism *J. Eur. Opt. Soc.—Rapid* **2** 07032
[19] Urbach H P and Pereira S F 2008 Field in focus with a maximum longitudinal electric component *Phys. Rev. Lett.* **100** 123904
[20] Török P 2003 An imaging theory for advanced, high numerical aperture optical microscopes *DSc Thesis* Hungarian Academy of Sciences
[21] Foreman M R and Török P 2010 Computational methods in vectorial imaging *J. Mod. Opt.* **58** 339–64
[22] Devaney A J and Wolf E 1974 Multipole expansions and plane wave representations of the electromagnetic field *J. Math. Phys.* **15** 234–44
[23] Wolf E 1959 Electromagnetic diffraction in optical systems. I. An integral representation of the image field *Proc. R. Soc.* A **253** 349–57
[24] Ignatowsky V S 1919 Diffraction by a lens of arbitrary aperture *Trans. Opt. Inst. Pet.* **1** 1–36
[25] Watson G N 1995 *A Treatise on the Theory of Bessel Functions* (Cambridge: Cambridge University Press)
[26] Rodríguez-Herrera O G, Lara D, Bliokh K Y, Ostrovskaya E A and Dainty C 2010 Optical nanoprobing via spin–orbit interaction of light *Phys. Rev. Lett.* **104** 253601